Catalysis Today 149 (2010) 240–247

Contents lists available at ScienceDirect

Catalysis Today

journal homepage: www.elsevier.com/locate/cattod

Novel supports for nickel-based catalysts for the partial oxidation of methane

Guillermo Paternina Berrocal [a], Andre L. M. Da Silva [b], José M. Assaf [b], Alberto Albornoz [c], Maria do Carmo Rangel [a,*]

[a] GECCAT, Instituto de Química, Universidade Federal da Bahia. Rua Barão de Geremoabo, s/n, Campus Universitário de Ondina, Federação, 40170-290, Salvador, Bahia, Brazil
[b] Laboratório de Catalise, Departamento de Engenharia Química, Universidade Federal de São Carlos, São Paulo, Brazil
[c] Centro de Química, Instituto Venezolano de Investigaciones Cientificas – IVIC, 21827, Caracas, Venezuela

ARTICLE INFO

Article history:
Available online 21 July 2009

Keywords:
Partial oxidation of methane
Syngas
Hydrogen
Zirconia
Nickel
Aluminum

ABSTRACT

Zirconia-supported nickel catalysts with different amounts of aluminum (Al/Zr = 0.2, 1 and 2) were studied in this work in order to find alternative supports for nickel-based catalysts for the partial oxidation of methane. This reaction is a promising route for producing hydrogen and syngas for different applications. Samples were prepared by precipitation and impregnation techniques, characterized by several techniques and evaluated in the partial oxidation of methane in the range of 450–750 °C and 1 atm. It was found that aluminum affects the textural and catalytic properties of zirconia-supported nickel catalysts. The tetragonal phase of zirconia was stabilized by aluminum and gamma-alumina was also found in the aluminum-richest samples. Aluminum increased the porosity and the specific surface area of the solids. The catalytic activity also increased with the amount of aluminum in solids probably due to the stronger interaction of nickel with the support, which slowly generates active sites during the reduction step. The methane conversion and hydrogen selectivity increased with temperature, indicating no deactivation. The hydrogen to carbon monoxide molar ratio decreased due to aluminum but was not significantly affected by temperature. The coke produced was not harmful to the catalysts and aluminum affected its amount, although no simple relationship was found between these parameters. The most promising catalyst was the sample with aluminum to zirconium molar ratio of 2, which showed high activity and hydrogen selectivity and was stable under the reaction condition.

1. Introduction

Hydrogen has attracted growing attention in last years since it has emerged as an alternative clean energy source to existing fossil fuels, besides its traditional use in chemical industries as well as in petroleum refineries. Today, its refinery use is the main contributor to new hydrogen plants at larger capacities, which is driven by environmental regulations requiring deeper desulphurization and fewer aromatics in fuels [1,2]. Hydrogen is also produced in large amounts for the manufacturing of ammonia or methanol and in GTL processes. In addition, its utilization in fuel cells is expected to increase in a near future; in special, hydrogen fuelled automotive sector could result in a large demand for new hydrogen production capacity [1].

The steam reforming process is the oldest and most widely used technology for producing hydrogen and syngas from hydrocarbon feedstock. However, this process requires a large energy input and high capital costs for maintaining the reaction conditions of superheated steam, high temperatures and pressures [3]. In addition, it provides a syngas with a too high H_2/CO ratio (>3) for the methanol and Fischer–Tropsch syntheses and the water gas shift reaction produces significant amounts of carbon dioxide in the product gas. The deactivation of nickel-based catalysts by coke is another drawback [3,4]. Also, it has a disadvantage of slow start-up, which does not make it suitable for mobile systems, such as fuel cells [3,5].

A promising route for overcoming these limitations is the partial oxidation of methane to syngas, which is more energy efficient, potentially more selective and yields a more suitable H_2/CO ratio for methanol and Fischer–Tropsch processes [3,4,6,7]. This reaction (Eq. (1)) is mildly exothermic, which is of particular importance for fuel cells [3,8–10].

$$CH_4 + 1/2O_2 \rightarrow CO + 2H_2 \qquad \Delta H^{\circ}_{298K} = -35.7\,kJ\,mol^{-1} \qquad (1)$$

It is commonly reported two classical reaction mechanisms to account for the partial oxidation of methane. The first one comprises the initial methane combustion (Eq. (2)) to produce carbon oxides and water, followed by steam or carbon dioxide reforming (Eqs. (3) and (4)) and the water gas shift reaction (Eq. (5)) to give the synthesis gas. The second mechanism is direct

* Corresponding author.
E-mail address: mcarmov@ufba.br (M.d.C. Rangel).

0920-5861/$ – see front matter © 2009 Elsevier B.V. All rights reserved.
doi:10.1016/j.cattod.2009.06.005

course, as shown in Eq. (1) [10–12]. However, some authors [13–15] claim that different pathways for hydrogen and carbon monoxide should be considered also. Horn et al. [14], for instance, have shown that even when the reaction proceeds via a direct partial oxidation (Eq. (1)) the hydrogen formation is not necessarily the primary event after methane dissociation at the catalyst surface. It is possible that the surface hydrogen atoms are involved in rapid surface reactions with surface oxygen atoms before they leave the surface as hydrogen or water. In this sense, the reaction would be indirect even through it follows Eq. (1). In this case, dry reforming (Eq. (4)) was not observed and hydrogen and carbon monoxide would be produced by partial oxidation (Eq. (1)) and partially by steam reforming (Eq. (5)). Liu et al. [15] have not observed the occurrence of dry reforming either and have proposed that the reaction mechanisms are different for the carbon and hydrogen components. They described a mechanism in which the overall reaction is dominated by the interplay between the direct oxidation of methane with oxygen to carbon monoxide and water and the subsequent reforming of methane with water. In this case, the total oxidation of carbon dioxide and water and the water gas shift reaction occur to a minor degree. On the other hand, Lyubovsky et al. [13] have found that hydrogen and syngas can also be produced via partial oxidation of methane in gas phase.

$$CH_4 + 2O_2 \rightarrow CO_2 + 2H_2O \qquad \Delta H^\circ_{298K} = -802.3\ \text{kJ mol}^{-1} \qquad (2)$$

$$CH_4 + H_2O \rightleftarrows CO + 3H_2 \qquad \Delta H^\circ_{298K} = +226\ \text{kJ mol}^{-1} \qquad (3)$$

$$CH_4 + CO_2 \rightleftarrows 2CO + 2H_2 \qquad \Delta H^\circ_{298K} = +261\ \text{kJ mol}^{-1} \qquad (4)$$

$$CO + H_2O \rightleftarrows CO_2 + H_2 \qquad \Delta H^\circ_{298K} = -41.2\ \text{kJ mol}^{-1} \qquad (5)$$

A number of catalysts have proven to be active in this reaction, mainly platinum group metals on various supports, such as rhodium, ruthenium, palladium, platinum and iridium [16,17], besides nickel and cobalt [3,17,18]. Some pyrochlore-type oxides, like $Ln_2Ru_2O_7$ [19] and perovskite type oxides with or without noble metals [9,20,21] have also been tested. Among these catalysts, noble metals are more active and have been widely used [22]; however, the high price of such systems limits their widespread industrial application. Nickel is an inexpensive metal but shows a tendency of sintering and needs to be stabilized [22]; in addition, it rapidly goes on deactivation by coke deposition [23,24].

Several strategies have been proposed to overcome these drawbacks. Many additives were successful used to decrease carbon deposition such as lithium, lanthanum, potassium, sodium, magnesium and calcium [25–27] as well as different methods to prepare the catalysts [28,29]. The use of different supports with basic sites, like calcium oxide, silica, magnesia [30], lanthana [31,32] and calcium phosphate/hydroxyapatite [33,34] or reducible supports [35,36] was also reported. Pure supports, such as ceria and zirconia, have been shown to be especially efficient for decreasing coke deposition by carbon gasification due to their oxygen storage capacity [37]. However, the high costs of these supports make their use unviable for commercial applications and then several works [38,39] have been carried out aiming to combine these materials with low cost materials such alumina.

With this goal in mind, this work deals with the preparation, characterization and evaluation of zirconia-supported nickel with several amounts of aluminum, in order to get more economic catalysts than those based on pure zirconia and more efficient than the alumina-based ones.

2. Experimental

2.1. Samples preparation

Samples with aluminum to zirconium molar ratio of 0.2, 1 and 2 (named AZ02, AZ1 and AZ2 samples, respectively) and pure zirconia (Z sample) were prepared by precipitation followed by calcination. In the zirconia preparation, a zirconium oxychloride (Merck) solution (1 M, 250 mL) and an ammonium hydroxide (Synth) solution (8.2%, v/v, 250 mL) were added to water (50 mL), under stirring at room temperature. The final value of pH was 9. The precipitated was aged for 48 h and centrifuged. The gel was then rinsed with an ammonium hydroxide solution (1%, v/v, 600 mL), dried at 120 °C for 24 h and then calcined at 500 °C, for 2 h, under air (20% O_2, 80% N_2, White Martins) flow. In order to prepare the zirconium and aluminum-containing solids, the same method was used but adding an aluminum nitrate (Synth) solution simultaneously with the zirconium oxychloride solution to water. In order to obtain solids with aluminum to zirconium molar ratio of 0.2, 1 and 2, 250 mL of 0.2, 1.0 and 1.0 of aluminum nitrate solutions and 250 mL of 1.0, 1.0 and 0.5 M of zirconium oxychloride solutions respectively, were used.

The supports thus obtained were impregnated with a nickel nitrate (Vetec) solution (2.5 M, 1.4 mL) in order to obtain 8% of the metal in final solids. During impregnation, the suspension was kept under stirring for 24 h, at room temperature and then the solid was separated by filtration, dried at 120 °C (24 h) and calcined at 550 °C, for 2 h. The presence of nickel in solids was indicated by the letter N. The calcination temperatures, for the supports and for the catalysts, were chosen from TG and DTA curves.

2.2. Samples characterization

The support precursors were characterized by differential thermal analysis (DTA), thermogravimetry (TG) and Fourier transform infrared spectroscopy (FTIR) and the supports were analyzed also by X-ray diffraction and nitrogen porosimetry. The fresh catalysts were characterized by these techniques and also by chemical analysis, temperature-programmed reduction and X-ray photoelectron spectroscopy. After reaction, the spent catalysts were characterized by the measurement of carbon content in order to quantify the coke deposited on the catalysts.

During the differential thermal analysis and thermogravimetry experiments, the sample (0.005 g) was heated at 10 °C min^{-1}, under air (20% O_2, 80% N_2, White Martins) flow from 30 to 1000 °C, in a Metter Toledo model TGA/SDTA851 equipment. These experiments were carried out on support precursors and on catalyst precursors (after nickel impregnation) in order to state the calcination temperature for the supports and for the catalysts, respectively. The presence of nitrate and chloride species in the samples was detected by FTIR, using a PerkinElmer model Spectrum One equipment, in the range of 400–4000 cm^{-1}. The samples were prepared as potassium bromide discs, in a 1:10 proportion. The metal contents in the solids were determined by X-ray dispersive energy in a Shimadzu model EDX-700HS equipment.

X-ray diffractograms were obtained using a model Shimadzu XRD600 equipment with a nickel filter. The sample was exposed to CuKα radiation (λ = 1.5420 Å) and then a scanning (2° min^{-1}) in the range of 2θ of 10–80° was carried out. The stability of the catalysts upon heating was monitored by getting X-ray diffractograms at different temperatures (650, 750, 850, 950, 1050 and 1150 °C), after heating the samples in situ in a chamber. The solids were heated at a rate of 10° min^{-1} under air (20% O_2, 80% N_2, White Martins) flow (100 mL min^{-1}) up to the desired temperature and the spectrum was registered. This procedure was repeated at each temperature.

The specific surface area (BET method) and porosity measurements were performed in a model ASAP 2020 Micromeritics apparatus on 0.30 g of sample, which was heated under vacuum (10 μmHg) at 200 °C for 30 min and then to 1 μmHg, before the nitrogen (99.999%, White Martins) adsorption.

Temperature-programmed reduction profiles were obtained using a Micromeritics model TPD/TPR 2900 equipment. In the analyses, the catalyst (0.30 g) was placed into a quartz cell and heated under nitrogen (99.999%, White Martins) flow (30 mL min^{-1}) up to 160 °C, at a rate of 10 °C min^{-1} and kept at this temperature for 30 min. The sample was then cooled to room temperature and heated again at a rate of 10 °C min^{-1} up to 1000 °C, under a 5% H_2/N_2 (White Martins) flow mixture (60 mL min^{-1}).

The XPS spectra were acquired with a VG Scientific spectrometer, Escalab model 220i-XL, with source of X-rays, MgKα (1253 eV) anode and 4000 W power and hemispheric electron analyzer. The Al 2p peak (BE = 74.5 eV) was chosen as an internal reference. This reference was in all cases in good agreement with the BE of the C 1s peak, arising from contamination, at 284.6 eV. This reference gives an accuracy of ±0.1 eV.

2.3. Catalytic evaluation

The partial oxidation of methane was carried out using a fixed bed continuous flow reactor loaded with 0.05 g of catalyst and a constant gas flow rate (40 mL min^{-1}) of methane (99.5%, Linde) and a mixture (94 mL min^{-1}) of oxygen diluted in nitrogen (20% O_2, 0.3% H_2O, N_2 balance, Linde), resulting in fluxes of 1.64×10^{-3} mol min^{-1} of methane and 0.8×10^{-3} mol min^{-1} of oxygen. The experiments were performed at temperatures of 750, 650, 550 and 450 °C in this order and at 1 atm. In order to study the catalysts stability, samples were evaluated at 700 °C, for 6 h. In all cases, oxygen was completely consumed. Prior to the experiments, the samples were reduced in situ at 600 °C, for 2 h under hydrogen (99.995%, Linde) flow (60 mL min^{-1}). Because of the small size of the catalytic bed and of the small particles size of the catalyst thermal gradients and external resistance to mass transfer are expected to be minimized and can be considered as negligible. In order to measure the amount of coke deposited on the catalysts, the carbon content in the spent catalysts was determined in a Leco model CS-200 equipment, using Lecocel and the iron chip accelerator.

3. Results and discussion

Table 1 shows the results of the chemical analysis of the catalysts. As a whole, the Al/Zr molar ratios were close to the expected ones, indicating an appropriate precipitation of aluminum and zirconium compounds. However, the sample with the lowest amount of aluminum (NAZ02) showed a lower value, indicating that the precipitation of zirconium compounds was favored as compared to aluminum compounds. For all samples the amount of nickel was lower than 8%, indicating that some nickel was lost during filtration.

Table 1
Chemical composition of the catalysts. NZ sample: pure zirconia-supported nickel. NAZ02, NAZ1 and NAZ2 samples: zirconium and aluminum compound-supported nickel with Al/Zr (molar) = 0.2, 1 and 2, respectively.

Sample	Al/Zr (molar) (expected)	Al/Zr (molar) (±0.07) (experimental)	Nickel amount (%) (±0.07)
NZ	–	–	6.04
NAZ02	0.2	0.13	6.34
NAZ1	1.0	1.22	6.73
NAZ2	2.0	2.04	6.89

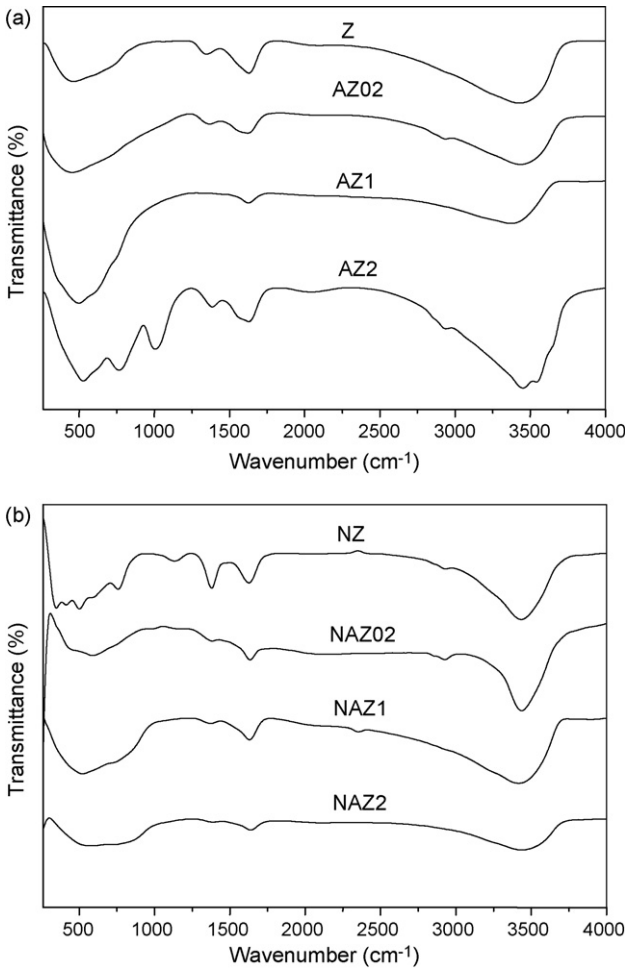

Fig. 1. FTIR spectra for the (a) supports before calcination and for the (b) catalysts after calcination. Z sample: pure zirconia precursor. AZ02, AZ1 and AZ2 samples: zirconium and aluminum compounds with Al/Zr (molar) = 0.2, 1 and 2, respectively. N represents the presence of nickel in solids.

The FTIR spectra for the support precursors and for the catalysts (Fig. 1) showed a broad band in the range of 3100–3400 cm^{-1} and a weak band at 1640 cm^{-1}, assigned to stretching and deformation vibrations of the water molecule, respectively [40]. Besides, a band at 1380 cm^{-1} is noticed (except for the AZ1 sample) which is typical of the nitrate or chloride species [41], indicating that the rinsing of the precipitate was not enough to remove these groups. The intensity of these bands decreased with calcination (Fig. 1b) but some nitrate species (probably from nickel nitrate) remained in the solids as we can see in the spectra of the catalysts. For all samples a broad band with several shoulders below 1000 cm^{-1} was noted, which is characteristic of Al–O and Zr–O vibrations [42–44]. For the AZ2 sample, a band 1020 cm^{-1} was also detected, characteristic of the deformation vibrations of water molecules in bohemite [43,44].

From the X-ray diffractograms (Fig. 2a), the monoclinic and tetragonal phases of zirconia (JCPDS 17-0923 and 37-1484) were identified in the support without aluminum (Z sample). The addition of aluminum caused the peaks enlargement, a fact that can be related to the production of small particles, related to the tetragonal zirconia, as claimed by previous workers [45]. The addition of higher amounts of aluminum (Al/Zr = 1 and 2) led to the production of gamma-alumina (JCPDS 48-0367). The diffraction profiles of the solids did not change after the addition of nickel as shown in Fig. 2b. Nickel oxide could not be identified in the catalysts because of the coincidence of the peak with that of the tetragonal phase of zirconia.

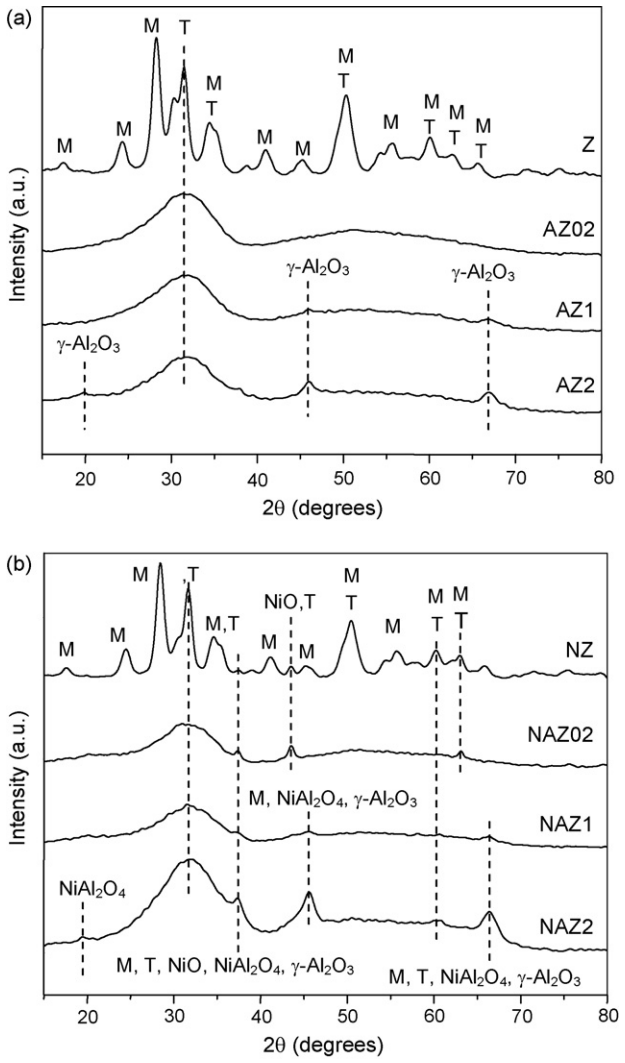

Fig. 2. X-ray diffractograms for the (a) supports and for the (b) catalysts. Z sample: pure zirconia. AZ02, AZ1 and AZ2 samples: zirconium and aluminum compounds with Al/Zr (molar) = 0.2, 1 and 2, respectively. N represents the presence of nickel in solids.

Nickel aluminate (JCPDS 10-0339) was identified by a peak at $2\theta = 19.20^{\circ}$ ($d = 4.61$ Å), which differed from that of gamma-alumina ($2\theta = 19.82^{\circ}$, $d = 4.47$ Å).

In order to identify the phases in the amorphous solids, additional experiments of X-ray diffraction were carried out upon heating in situ. For all solids, the peaks got narrower upon heating allowing to relate them to the amorphous halos, detected at room temperature, with crystalline phases. Fig. 3 illustrated the X-ray diffractograms of zirconia-supported nickel (NZ) and of an aluminum-containing catalyst (NAZ1) performed at different temperatures. In the first case, peaks related to the tetragonal and monoclinic phases of zirconia were noted and nickel oxide could be identified at 650 °C. For the NAZ1 sample only the tetragonal phase, stabilized by aluminum, was detected. For this sample, the peaks assigned to gamma-alumina were coincident with those of the tetragonal phase and/or with those of nickel compounds and then this phase could not be identified. Again, no peak related to nickel compounds could be identified.

The production of nickel oxide was confirmed by thermogravimetry, carried out on the samples after nickel impregnation and before calcination. Fig. 4 shows the curves of derivative thermogravimetry of the catalysts. The curves showed a weight loss in two steps: the first, in the range of 25–170 °C, corresponds to the loss of water and volatile materials adsorbed on solids while the other (200–450 °C) is related to the production of nickel oxide from nickel nitrate. According to previous work [46], there are several weight losses during the decomposition of nickel nitrate, related to intermediate products, which make difficult the identification of the formation of each product. In spite of this fact, a weight loss between 260 and 380 °C fits well with to the theoretical weight loss due to the transformation of nickel nitrate to nickel oxide and then can be assigned to this process.

The specific surface areas of the supports and of the catalysts are shown in Table 2. It can be noted that the addition of aluminum caused a significant increase in the specific surface area of zirconia and this effect increased with the amount of aluminum in solids; therefore the aluminum-richest sample (AZ2) showed the highest value. By adding nickel to the solids the specific surface area decreased, around 15–26%, but no regular tendency was noted between this decrease and the amount of aluminum in solids. This can be assigned to the sinterization of solids during calcination, after nickel impregnation, in agreement with previous work [47] and to the partial blockage of the pores by nickel oxide particles. The specific surface areas of the catalysts changed with aluminum amount in a similar tendency noted with the supports and thus the aluminum-richest sample showed the highest value.

From the experiments of nitrogen adsorption, isotherms with different profiles were obtained, as shown in Fig. 5. For both supports and catalysts, these curves can be considered as variations of Type III isotherms with a loop of hysteresis, which is typical of macroporous materials with mesopores [48]. It can be noted that the addition of aluminum to zirconia increased the porosity of the solids by creating smaller mesopores that adsorbed nitrogen at lower pressures. The same behavior was noted for the catalysts, the aluminum-containing samples showed smaller mesopores, indicating that aluminum increased the porosity of the catalysts. The largest amount of small mesopores was displayed by the sample with Al/Zr = 1 (NAZ1), which showed the widest loop of hysteresis at low pressure. Table 2 shows the average pore diameter and pore volume of the solids. There was a decrease of the average pore diameter of the supports which can explain the increase of specific surface areas due to aluminum The addition of nickel caused a slight decrease of average pore volume, probably due to the partial blockage of the pores, causing a decrease in the specific surface area.

The TPR curves for the samples are shown in Fig. 6. Zirconia-supported nickel (NZ) showed two overlapped peaks at 353 and 509 °C, which are assigned to the reduction of nickel species in different kinds of interaction with the support, in agreement with previous work [47,49]. The peak at low temperature (300–400 °C) is related to the reduction of large nickel oxide particles [50,51], whereas the high temperature one (400–700 °C) is associated to the reduction of highly dispersed nickel oxide in interaction with the support [50]. These peaks were shifted to higher temperature due to the addition of aluminum in solids and this effect increased with its amount in solids, as we can see in Fig. 6, suggesting that nickel oxide is more dispersed in these samples. For the catalyst with the highest amount of aluminum (NAZ2) the broad peak was shifted at even higher temperatures (around 800 °C), suggesting that some highly dispersed nickel oxide has formed nickel aluminate, which is less reducible [49–51].

The binding energies (BE) of some characteristic core levels of zirconium, aluminum, oxygen and nickel for the fresh catalysts are displayed in Table 3. The binding energies for the Zr $3d_{5/2}$ peak are in close agreement with those for Zr^{4+} in ZrO_2-type compounds [52] and in accordance with previous work [53]. The binding energy for the Al 2p peak showed a value typical of Al^{3+} in $Al_2O_4^{2-}$ type compounds [52]. The most intense Ni $2p_{3/2}$ peak, which appears at around 855.6 eV for zirconia-supported nickel is

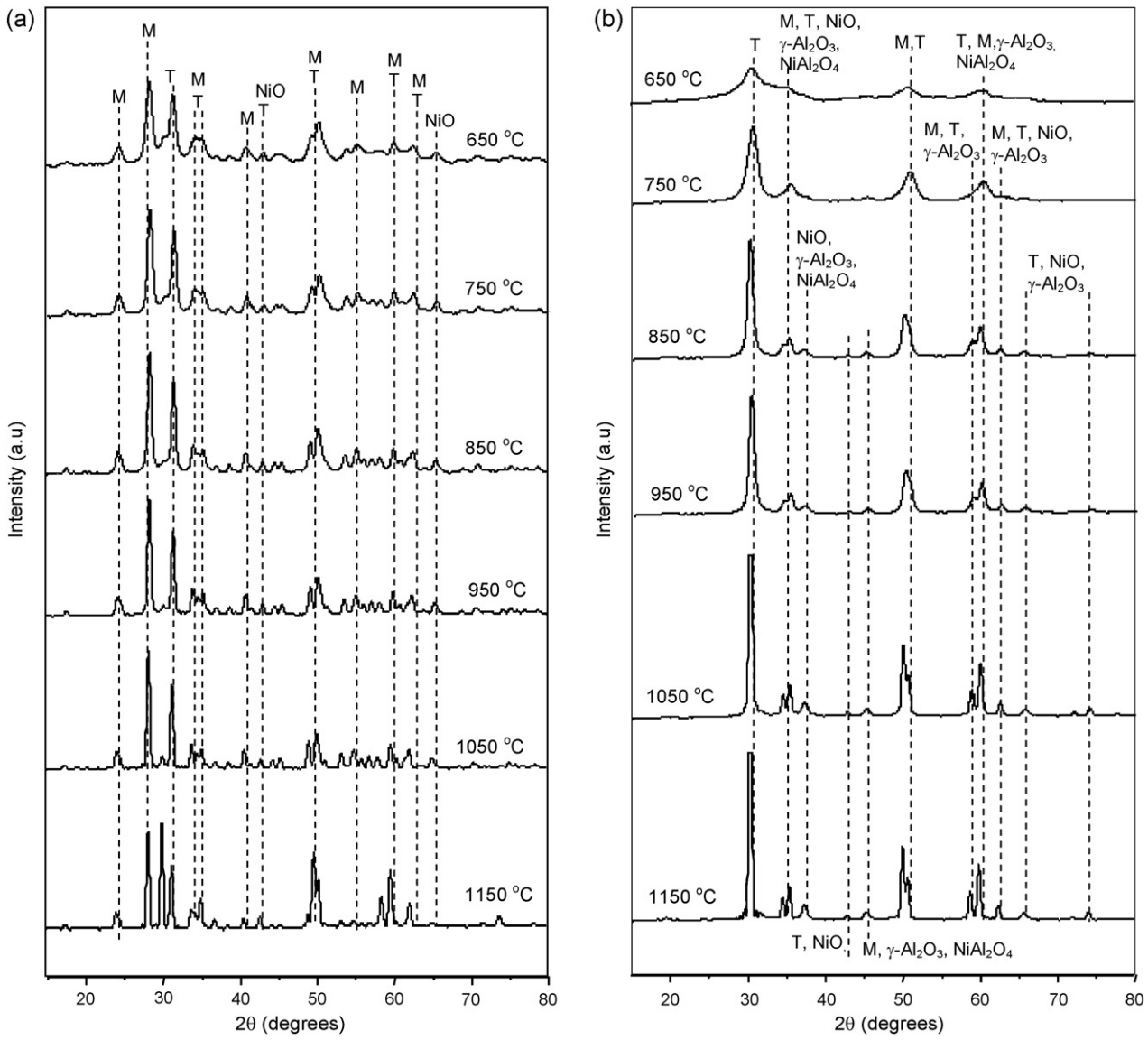

Fig. 3. X-ray diffractograms for the (a) NZ (zirconia-supported nickel) and (b) NAZ1 (zirconium and aluminum compound-supported nickel with Al/Zr (molar) = 1) samples, obtained at different temperatures. M, monoclinic phase of zirconia; T, tetragonal phase of zirconia.

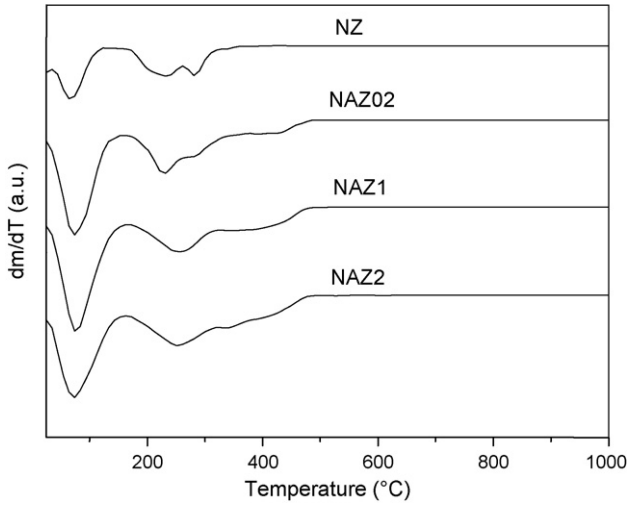

Fig. 4. Curves of derivative thermogravimetry for the catalysts before calcination. NZ sample: zirconia-supported nickel; NAZ02, NAZ1 and NAZ2 samples: zirconium and aluminum compounds-supported nickel with Al/Zr (molar) = 0.2, 1 and 2.

characteristic of Ni^{2+} ions in an oxygen environment and is accompanied by a satellite line positioned at ca. 6 eV on the higher BE side, this peak is related to nickel oxide [52,54]. The addition of small amounts of aluminum (NAZ02 and NAZ1 sample) did not cause any difference in this value; however higher amounts of aluminum (NAZ2 sample) led to higher values (around 856.0 eV) which is typical of nickel aluminate [54]. The same tendency was noted for the binding energy of core level of oxygen; for the NZ,

Table 2
Textural properties of the supports and of the catalysts. Z sample: pure zirconia. AZ02, AZ1 and AZ2 samples: zirconium and aluminum compounds with Al/Zr (molar) = 0.2, 1 and 2, respectively. N indicates the presence of nickel in solids.

Samples	Sg ($m^2\ g^{-1}$)	Average pore diameter (Å)	Average pore volume ($cm^3\ g^{-1}$)
Z	111	122	0.46
AZ02	222	85	0.60
AZ1	256	–	–
AZ2	282	50	0.42
NZ	95	154	0.45
NAZ02	171	93	0.53
NAZ1	187	43	0.29
NAZ2	210	59	0.39

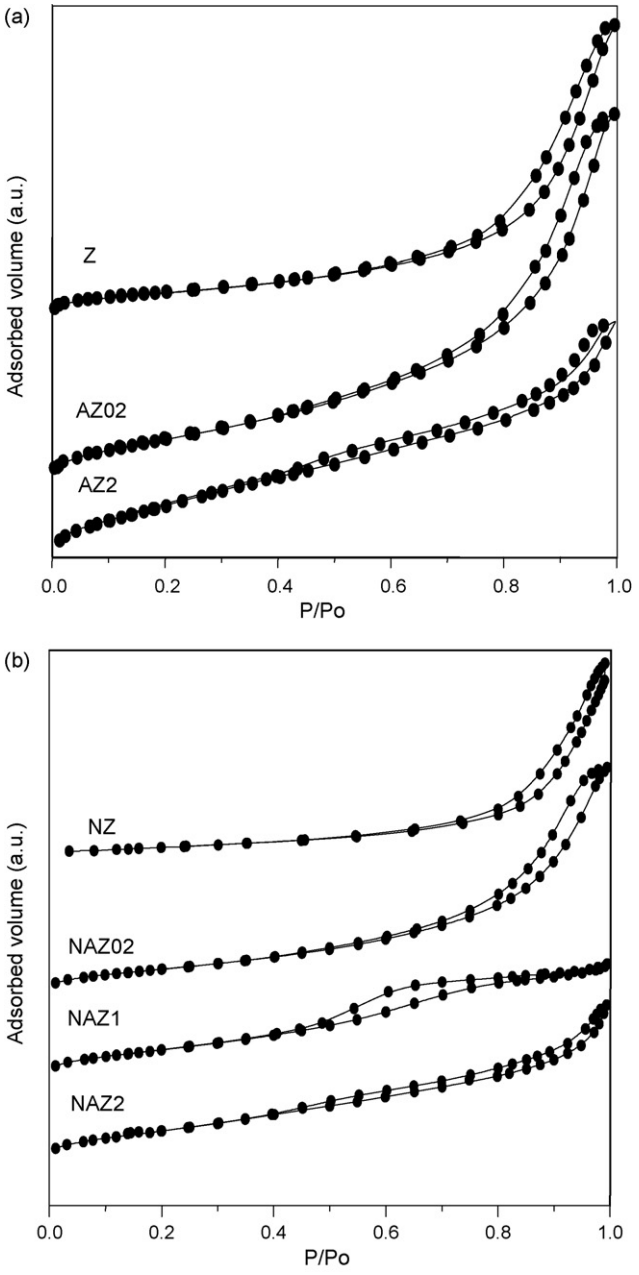

Fig. 5. Nitrogen isotherms for the (a) supports and for the (b) catalysts. Z sample: zirconia; AZ02 and AZ2 samples: zirconium and aluminum compounds with Al/Zr (molar) = 0.2 and 2. NZ sample: zirconia-supported nickel; NAZ02, NAZ1 and NAZ2 samples: zirconium and aluminum compound-supported nickel with Al/Zr (molar) = 0.2, 1 and 2.

NAZ02 and NAZ1 samples the values were close to that of nickel oxide while for the other sample it was close to the value of nickel aluminate [54]. As expected, the aluminum to zirconium molar ratio on the surface increases with the amount of aluminum on the solids, but no direct relationship between these parameters was found. It can also be noted that the amount of nickel on surface (measured by the Ni/(Zr + Al) molar ratio) increased with the metal content up to Al/Zr = 1 and then decreased with the increase of its amount in solids. Therefore, the solid with the highest amount of nickel on the surface was that with Al/Zr = 1 (NAZ1) and the sample with the lowest nickel on the surface was the aluminum-free solid.

The values of methane conversion and hydrogen selectivity as a function of temperature are shown in Table 4. All catalysts were active in this temperature range (450–750 °C), without deactivation

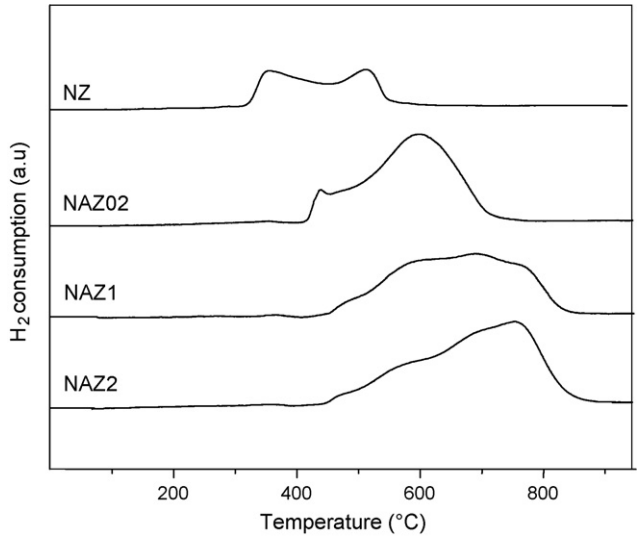

Fig. 6. TPR curves for the catalysts. NZ sample: zirconia-supported nickel; NAZ02, NAZ1 and NAZ2 samples: zirconium and aluminum compound-supported nickel with Al/Zr (molar) = 0.2, 1 and 2.

Table 3
Binding energy of core level of zirconium, aluminum, oxygen and nickel and surface composition of the samples. NZ sample: pure zirconia-supported nickel. AZ02, AZ1 and AZ2 samples: zirconium and aluminum compound-supported nickel with Al/Zr (molar) = 0.2, 1 and 2, respectively.

Amostra	Zr $3d_{5/2}$	Al 2p	O 1s	Ni 2p	Al/Zr	Ni/(Zr + Al)
NZ	181.8	–	529.9	855.6	–	0.09
NAZ02	181.9	73.5	529.9	855.4	0.25	0.18
NAZ1	181.5	74.0	530.4	855.7	1.37	0.25
NAZ2	181.6	74.3	530.6	856.0	1.41	0.14

in the reaction condition, the conversion continuously increased with temperature. Also, the methane conversion remains the same during 350 min at 700 °C, as shown in Fig. 7a.

It can be noted that the addition of aluminum increased the catalytic activity in the whole temperature range and this effect increased with the amount of this metal in solids; therefore, the richest-aluminum sample (NAZ2) was the most active catalyst. The effect of aluminum on the activity of the catalysts can be related to its role in increasing both the specific surface area and the interaction of nickel with the support. As the aluminum

Table 4
Methane conversion (X), hydrogen selectivity (S_{H_2}) and H_2/CO in the partial oxidation of methane as a function of temperature. NZ sample: pure zirconia-supported nickel. NAZ02, NAZ1 and NAZ2 samples: zirconium and aluminum compound-supported nickel with Al/Zr (molar)= 0.2, 1 and 2, respectively.

Sample		NZ	NAZ02	NAZ1	NAZ2
X (%)	450 °C	39	42	46	49
	550 °C	52	54	57	61
	650 °C	67	68	70	75
	750 °C	76	78	81	85
(S_{H_2}) (%)	450 °C	34	33	39	42
	550 °C	48	46	52	55
	650 °C	64	63	66	70
	750 °C	74	75	78	82
H_2/CO	450 °C	3.1	2.3	2.6	2.5
	550 °C	2.3	2.0	2.1	2.0
	650 °C	2.0	1.7	1.8	1.8
	750 °C	1.9	1.7	1.7	1.7
Coke (%)		26.5	40.9	16.9	23.6

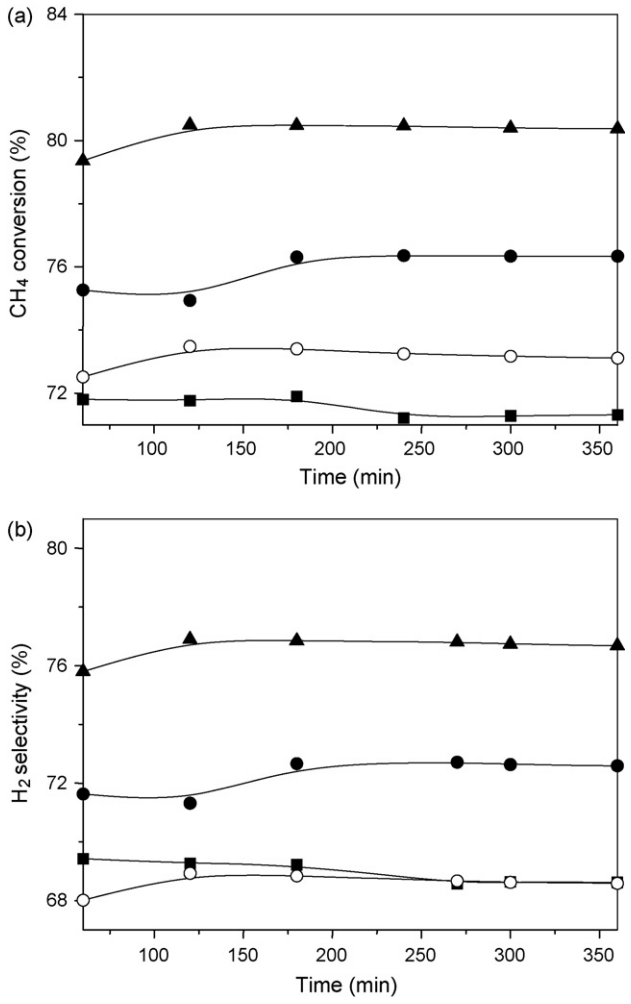

Fig. 7. Methane conversion (a) and hydrogen selectivity (b) as a function of time for the catalysts in the partial oxidation of methane. NZ sample (■): zirconia-supported nickel; NAZ02 (○), NAZ1(●) and NAZ2 (▲) samples: zirconium and aluminum compound-supported nickel with Al/Zr (molar) = 0.2, 1 and 2.

concentration in solids increased, the specific surface area (Table 2) and the nickel interaction with the support (Fig. 6) increased. As we can see from Table 3, the aluminum amount on the surface increased with its concentration in solids and then the aluminum-richest sample has the highest amount on the catalyst surface. Because of the tendency of nickel to react with aluminum [55] to form nickel aluminate, it is expected that the aluminum-richest sample has a large amount of this compound on the surface and then shows the highest activity. As pointed out earlier [47], the nickel aluminate phase promotes a slow reduction of the Ni^{2+} species and then leads to the generation of smaller and more active metallic sites during the reduction step, as compared to the metal particles originated from the reduction of nickel oxide. Although the aluminum-richest sample (NAZ2) has the smallest amount of nickel on the surface of the fresh catalyst, as compared to the other aluminum-containing samples, it has the highest amount of aluminum and then it is reasonable to consider that most of nickel is in strong interaction with the support, forming nickel aluminate. Therefore, during the reduction step, this sample is able to produce the smallest and most active metal particles, among the catalysts. In fact, from both the XPS and TPR results, the presence of nickel aluminate in this sample was suggested. These sites need a high temperature to be formed as shown by the TPR curves and then a slight activation is noted, from Fig. 7, which can be assigned to the production of new active sites coming from the reduction of nickel aluminate, during reaction.

The hydrogen selectivity also increased with temperature (Table 4) and the values were stable under the reaction condition as found in Fig. 7b. As a whole the selectivity slightly increased with the aluminum concentration. In the whole temperature range, the aluminum-richest sample (Al/Zr = 2) was the most selective one.

The H_2/CO ratio also changed with the amount of aluminum and with temperature but no simple relationship was found; in a general tendency, more carbon monoxide was detected as the amount of aluminum increased in the catalysts and then this ratio was decreased; therefore, zirconia-supported nickel showed the highest value of the H_2/CO ratio at all temperatures. This suggests that the combustion reaction (Eq. (2)), followed by steam reforming, dry reforming and the water gas shift reaction (Eqs. (3)–(5)) was favored over all catalysts. These results are in agreement with previous works [3,56], carried out with zirconia-supported nickel and alumina-supported nickel. Also, the water gas shift was inhibited by aluminum, the consumption of carbon monoxide was decreased over the aluminum-containing catalysts.

All catalysts produced high amounts of coke, as shown in Table 4 but it did not affect the catalytic performance during the 6 h of reaction, as shown in Fig. 7. From these results, it can be supposed that this carbon is probably of the filamentous-type and not of encapsulating-type which would cause a decrease in activity [57], as found by previous workers [58–61]. The aluminum amount affected coke deposition but no simple relationship was found between these two parameters.

4. Conclusions

The addition of aluminum to zirconia-supported nickel catalysts caused, in a range of Al/Zr = 0.2, 1 and 2, changes in their textural and catalytic properties. The tetragonal phase of zirconia was stabilized by aluminum and gamma-alumina phase was also found in the aluminum-richest samples. The specific surface areas increased with the aluminum amount in solids, this fact can be related to a decrease of the particles size (evidenced by the stabilization of the tetragonal zirconia) and also to an increase of porosity. The catalytic activity also increased due to aluminum probably due to an increase of the interaction of nickel with the support, which slowly generates active sites during the reduction step; this effect increased with the aluminum concentration in solids. All catalysts were active in the partial oxidation of methane and were selective towards hydrogen, in the range of 450–750 °C; they did not deactivate in these conditions. Aluminum also decreased the hydrogen to carbon monoxide molar ratio, which was not significantly affected by temperature. Coke produced during reaction was not harmful to the catalysts and aluminum affected its amount; however, no simple relationship was found between the aluminum content and coke amount. The most promising catalyst was the sample with aluminum to zirconium molar ratio of 2, which showed high activity and hydrogen selectivity, besides being stable under reaction condition.

Acknowledgments

GPB acknowledges CAPES and FAPESB for his graduate fellowship. The authors thank FINEP, CNPq and FAPESB for the financial support.

References

[1] T. Rostrup-Nielsen, Catal. Today 106 (2005) 293.
[2] R. Ramachandran, R.K. Menon, Int. J. Hydrogen Energy 23 (1998) 593.
[3] A.M. Diskin, R.M. Ormerod, Stud. Surf. Sci. Catal. 130 (2000) 3519.
[4] E. Ruckenstein, H.Y. Wang, J. Catal. 187 (1999) 151.
[5] Y.-S. Seo, A. Shirley, S.T. Kolaczkowski, J. Power Sources 108 (2002) 213.

[6] R. Lanza, S.G. Jaras, P. Canu, Appl. Catal. A: Gen. 325 (2007) 57.
[7] C. Guo, X. Zhang, J. Zhang, Y. Wang, J. Mol. Catal. A 269 (2007) 254.
[8] J.M. Fox, Catal. Rev. Sci. Eng. 35 (1993) 169.
[9] G.C. Araújo, S. de Lima, M.C. Rangel, V.L. Pagola, M.A. Peña, J.L.G. Fierro, Catal. Today 107 (2005) 906.
[10] R. Lødeng, E. Bjørgum, C. Bjørn, J. Eilertsen, A. Holmen, M.R. Krogh, E. Rytter, Appl. Catal. A: Gen. 333 (2007) 11.
[11] K. Nakagawa, N. Ikenaga, T. Kobayashi, T. Suzuki, Catal. Today 64 (2001) 31.
[12] S.C. Tsang, J.B. Claridge, M.L.H. Green, Catal. Today 23 (1995) 3.
[13] M. Lyubovsky, H. Karim, P. Menacherry, S. Boorse, R. LaPierre, S. Roychoudhury, Catal. Today 83 (2003) 183.
[14] R. Horn, K.A. Williams, N.J. Degenstein, A. Bitsch-Larsen, D. Dalle Nogare, S.A. Tupy, L.D. Schmidt, J. Catal. 249 (2007) 380.
[15] T. Liu, C. Snyder, G. Veser, Ind. Eng. Chem. Res. 46 (2007) 9045.
[16] M.C.J. Bradford, M.A. Vannice, Catal. Today 50 (1999) 87.
[17] P.M. Torniainen, X. Chu, L.D. Schmidt, J. Catal. 146 (1994) 1.
[18] C.T. Au, H.Y. Wang, J. Catal. 167 (1997) 337.
[19] R.H. Jones, A.T. Ashcroft, D. Waller, A.K. Cheetham, J.M. Thomas, Catal. Lett. 8 (1991) 169.
[20] V.R. Choudhary, B.S. Uphade, A.A. Belhekar, J. Catal. 163 (1996) 312.
[21] S. Cimino, G. Landi, L. Lisi, G. Russo, Catal. Today 117 (2005) 718.
[22] S. Freni, G. Calogero, S. Cavallaro, J. Power Sources 87 (2000) 28.
[23] S. Pengpanich, V. Meeyoo, T. Rirksomboon, Catal. Today 93–95 (2004) 95.
[24] J. Barbero, M.A. Peña, J.M. Campos-Martin, J.L.G. Fierro, P.L. Arias, Catal. Lett. 87 (2003).
[25] Q. Miao, G. Xiong, S. Sheng, W. Cui, L. Xu, X. Guo, Appl. Catal. A: Gen. 154 (1997) 17.
[26] J. Requies, M.A. Cabrero, V.L. Barrio, M.B. Güemez, P.L. Arias, M.A. Peña, V. La Parola, J.L.G. Fierro, Catal. Today 116 (2006) 304.
[27] F. Basile, G. Fornasari, F. Trifirò, A. Vaccari, Catal. Today 64 (2001) 21.
[28] S. Xu, R. Zhao, X. Wang, Fuel Proc. Technol. 86 (2004) 123.
[29] Y. Zhang, G. Xiong, S. Sheng, W. Yang, Catal. Today 63 (2000) 517.
[30] S. Tang, J. Lin, K.L. Tan, Catal. Lett. 51 (1998) 169.
[31] A. Slagtern, U. Olsbye, Appl. Catal. A: Gen. 110 (1994) 99.
[32] V.A. Tsiapouriari, Z. Zhang, X.E. Verykios, J. Catal. 179 (1998) 283.
[33] J.H. Jun, T.-J. Lee, T.H. Lim, S.-W. Nam, S.-A. Hong, K.J. Yoon, J. Catal. 221 (2004) 178.
[34] J.H. Jun, T.H. Lim, S.-W. Nam, S.-A. Hong, K.J. Yoon, Appl. Catal. A: Gen. 312 (2006) 26.
[35] P. Pantu, G.R. Gavalas, Appl. Catal. A: Gen. 223 (2002) 253.
[36] T. Wu, Q. Yan, H. Wan, J. Mol. Catal. A: Chem. 226 (2005) 41.
[37] H.S. Roh, H.S. Potdar, K.W. Jun, Catal. Today 93 (2004) 39.
[38] H.S. Roh, K.W. Jun, S.E. Park, Appl. Catal. A: Gen. 251 (2003) 275.
[39] Y.S. Oh, H.S. Roh, K.W. Jun, Y.S. Baek, Int. J. Hydrogen Energy 28 (2003) 1387.
[40] B. Stuart, B. George, P. McIntyre, Modern Infrared Spectroscopy, Ed. John Wiley & Sons Ltd., England, 1996.
[41] R.A. SyQuest, R.O. Bagel, Infrared Spectra of Inorganic Compounds, Academic Press, Orlando, 1971.
[42] S.H. Yariv, E. Mendelovici, Appl. Spectrosc. 33 (1979) 410.
[43] D. Mishra, S. Anand, R.K. Panda, R.P. Das, Mater. Lett. 42 (2000) 38.
[44] I.H. Joe, G.A. A.D. Damodaran, K.G.K. Warrier, J. Solid State Chem. 131 (1997) 181.
[45] R.C. Garvie, J. Phys. Chem. 69 (1965) 1238.
[46] J. Estellé, P. Salagre, Y. Cesteros, M. Serra, F. Medina, J.E. Sueiras, Solid State Ionics 156 (2003) 233.
[47] S.P. de Lima, V. Vicentini, J.L.G. Fierro, M.C. Rangel, Catal. Today 133–35 (2008) 925.
[48] P.A. Webb, C. Orr, Analytical Methods in Fine Particle Technology, Micromeritics Instruments Coorporation, Norcross, 1997.
[49] F. Pompeo, D. Gazzoli, N. Nichio, Int. J. Hydrogen Energy 34 (2009) 2260.
[50] A.M. Diskin, R.H. Cunningham, R.M. Ormerod, Catal. Today 46 (1998) 147.
[51] Y. Xie, Y. Tang, Adv. Catal. 37 (1990) 1.
[52] C. D. Wagner, W.N. Riggs, L.E. Davis, J. F. Moulder, Handbook of X-Ray Photoelectron Spectroscopy, PerkinElmer, Eden Praire, 1979.
[53] S. Ardizone, C.L. Bianch, E. Grassi, Colloids Surf. 135 (1998) 41.
[54] G.R. Gavalas, C. Phichitkul, G.E. Voecks, J. Catal. 88 (1984) 54.
[55] Y. Lu, J. Xue, C. Yu, Y. Liu, S. Shen, Appl. Catal. A: Gen. 174 (1998) 259.
[56] M.E.S. Hegarty, A.M. ÓConnor, J.R.H. Ross, Catal. Today 42 (1998) 225.
[57] D.L. Trimm, Catal. Today 49 (1999) 3.
[58] G.C. Araújo, S.M. de Lima, J.M. Assaf, M.A. Peña, J.L.G. Fierro, M.C. Rangel, Catal. Today 133–135 (2008) 129.
[59] Y. Li, J. Chen, Y. Qin, L. Chang, Energy Fuels 14 (2000) 1188.
[60] Y. Li, B. Zhang, X. Xie, J. Liu, Y. Xu, W. Shen, J. Catal. 238 (2006) 412.
[61] K. Murata, M. Inaba, M. Miki, T. Yamaguchi, React. Kinet. Catal. Lett. 85 (2005) 21–27.